JOURNAL OF GEOPHYSICAL RESEARCH, VOL. 103, NO. B2, PAGES 2501–2514, FEBRUARY 10, 1998

Thermodynamics of lateral dike propagation: Implications for crustal accretion at slow spreading mid-ocean ridges

Yuri A. Fialko and Allan M. Rubin

Department of Geosciences, Princeton University, Princeton, New Jersey

Abstract. We consider solidification of hot fluid flowing through a rigid-wall channel of infinite extent. The calculated "thermal arrest" lengths are used to investigate the role of magma freezing in limiting the propagation distance of lateral dike intrusions. Our results demonstrate that for reasonable parameters the propagation distances of meter-wide dikes do not exceed the wavelength of crustal thickness variations or transform fault spacing along slow spreading ridges. This suggests that thermal controls on the crustal melt delivery system could be an important factor in modulating these variations. Unlike published results for a finite channel, which predict unlimited meltback of the channel walls if the prefreezing fluid velocity exceeds some critical value, any flow into an infinite channel will eventually freeze, provided that shear heating in the magma is negligible. The thermal arrest distances depend strongly on the average dike thickness h ($\propto h^4$ for dikes driven by an along-strike topographic slope and $\propto h^2$ for dikes driven by an excess source pressure). Thermal erosion of the country rocks associated with lateral dike intrusions is likely to be confined to a very small region near the magma source. Substantial correlations between the along-strike bathymetry and geochemistry of the erupted lavas along individual ridge segments may be consistent with high-level basalt fractionation in the laterally propagating dikes.

1. Introduction

It is generally recognized that tectonics and magmatism at constructive plate margins are intrinsically coupled. One well-known illustration of this is the strong modulation of the rate and mode of magma supply to the mid-ocean ridge (MOR) axis by the spreading rate. Thus mantle flow beneath fast spreading ridges is believed to be mainly two-dimensional, and the magma supply is robust and crustal magma chambers may exist over the whole length of ridge segments [e.g., *Sleep*, 1975; *Detrick et al.*, 1987]. As a result, a well-developed gabbroic layer (layer 3) is present in the crust along most of the ridge axis and along-strike variations in crustal thickness and topography are rather small. This seems to be the case for most of the East Pacific Rise (EPR) [*Lin and Phipps Morgan*, 1992]. In contrast, slow spreading ridges (such as most of Atlantic, Indian and Antarctic Ridges) are characterized by distinct magmatic and morphologic segmentation having a spatial wavelength of the order of 50 km [*Schouten et al.*, 1985; *Dick*, 1989].

Observational data characterizing typical slow spreading ridge segments can be summarized as follows. Magmatic centers are located roughly in the middle of ridge segments and are marked by topographic highs; typical segment half lengths are 15-35 km, and along-axis elevation drops from the central high to adjacent transform faults are of the order of 1 km [*Francheteau and Ballard*, 1983; *Neumann and Forsyth*, 1993]. Along-axis topography is inversely correlated with Bouguer gravity anomalies, which suggests a direct correlation between the surface topography and crustal thickness [*Lin et al.*, 1990]. Along-axis thinning of the oceanic crust away from the central high has been also inferred from seismic [*Mutter et al.*, 1985; *Tolstoy et al.*, 1993] and petrologic [*Dick*, 1989] data. At the same time, the thickness of the lithosphere, which is usually associated with the depth of some particular (~600°C) isotherm, is believed to increase toward the bounding transform faults. These along-strike variations are commonly ascribed to essentially three-dimensional quasi-regular asthenospheric upwellings [*Whitehead et al.*, 1984; *Lin and Phipps Morgan*, 1992]. While focused mantle upwelling may be a plausible cause of an increase in lithospheric thickness off of the upwelling center, shallow processes (e.g., magma migration within the lithosphere) may be important in producing the observed correlation between crustal thickness variations and segmentation pattern.

It has been suggested that crustal thinning is related to the along-strike thermal structure of ridge segments [e.g., *Lin et al.*, 1990], although the particular mechanisms of such thermal control are poorly understood. It is often assumed that melt transport at ridges is predominantly vertical and that the local crustal thickness reflects the accumulated thickness of magma extracted from a vertical cross section perpendicular to the ridge at that location [*Lin and Phipps Morgan*, 1992; *Cannat*, 1996]. At the same time, it has been proposed that crustal accretion at magma-starved mid-ocean ridge segments involves significant downrift melt transport from the central magma chamber via dikes and sills [e.g., *White*, 1989; *Bloomer et al.*, 1989]. Lateral dike propagation has been well documented by the observations in Iceland, in Hawaii, and on the Juan de Fuca Ridge [*Einarsson and Brandsdottir*, 1980; *Klein et al.*, 1987; *Fox et al.*, 1995]. If the role of lateral transport in the total magma budget of slow spreading ridge segments is significant, then the thermal viability of dikes is

Paper number 97JB03105.
0148-0227/98/97JB-03105$09.00

likely to be a major factor controlling the observed along-axis variations in crustal morphology. In this case, magma freezing during downrift flow could be responsible for the observed thinning of the ocean crust, either directly by limiting the magma supply or indirectly by allowing for tectonic thinning in the absence of magma input. However, it remains enigmatic why magma should have difficulty reaching the ends of small segments on a slow spreading ridge, which requires lateral propagation of some 15-20 km, while traveling up to 100 km along the Juan de Fuca Ridge [*Dziak et al.*, 1995] and in volcanic rift zones of Iceland and Hawaii [*Sigurdsson and Sparks*, 1978].

The role of magma freezing in limiting dike propagation distance has been addressed previously but not in the context of laterally propagating dikes. *Delaney and Pollard* [1982], *Bruce and Huppert* [1990], and *Lister and Dellar* [1996] considered constant-pressure-drop flow through a slot of specified thickness from a shallow magma source to the surface. While *Delaney and Pollard* [1982] postulated a priori that the solidification front always moved toward the dike center, *Bruce and Huppert* [1990] and *Lister and Dellar* [1996] included the possibility of melting the dike walls (meltback) in their models and found that thermal runaway (i.e., an infinite thermal erosion of the channel as long as the magma supply lasts) takes place in even relatively thin dikes (having thickness of ~1 m). This result is somewhat puzzling in that ample field data do not suggest any signs of meltback for such (and many thicker) dikes. The more recent solution of *Lister and Dellar* [1996], which is the only one of the above to solve the complete equations for the advection and diffusion of heat, might be expected to underestimate freezing if applied to laterally propagating dikes because of the following assumptions: (1) cooled magma simply flows onto the surface, instead of remaining in the dike channel where it may further impede the flow; (2) magma is emplaced in a finite-length channel instantaneously or on a timescale that is much shorter than the subsequent solidification; and (3) the thinner region near the propagating dike tip is absent. *Lister* [1994a,b] presents another analysis for vertically propagating dikes in which the dike walls are considered to be perfectly flexible. In this model, the flow is governed by the balance between buoyant and viscous forces and elasticity is neglected, so the dike walls respond passively to mass balance of the flow. The free deformability of the boundaries allows the chill to be displaced laterally and flow to continue if sufficient flux is arriving from the source [*Lister*, 1994b]. This assumption is not appropriate for laterally propagating dikes in which the thickness is constrained by elasticity everywhere.

In this paper we determine the thermal arrest length of laterally propagating dikes by considering time-dependent fluid flow in a rigid-walled channel of infinite extent, in which the phase transition between liquid and solid is assumed to occur at a specified temperature. In our calculations we explicitly incorporate a topographic (gravitational) component of the pressure gradient driving the flow, which, as we show below, may provide the dominant driving force for many mid-ocean ridge dikes. While the models discussed below are most obviously applicable to laterally propagating dikes fed by a shallow chamber, they are also applicable to dikes that rise directly from the mantle and begin to spread laterally within the crust. Such behavior has been shown experimentally and is predicted theoretically when the dike reaches either the level of neutral buoyancy (if the least horizontal compressive stress is essentially equal to the vertical stress; e.g. *Ryan* [1987]; *Lister and Kerr* [1991]), or a rheologically-controlled level such as the brittle/ductile transition (if the horizontal stress is modified significantly by tectonic extension [e.g., *Rubin*, 1990, 1995].

2. Preliminaries

We start by considering the behavior of a fluid-driven crack in the presence of a small topographic slope and a constant excess pressure p at the source (the excess pressure is defined as the difference between the magma pressure and the ambient dike-perpendicular stress). Figure 1 shows a schematic view of a dike driven by the release of an incompressible melt of density ρ_m from a source (origin in Figure 1) embedded in a stratified elastic half-space. The surface of the half-space is inclined by an angle α with respect to horizontal. Following *Rubin and Pollard* [1987] and *Lister* [1990], we assume that the level of "neutral buoyancy" (LNB) for the fluid tracks the half-

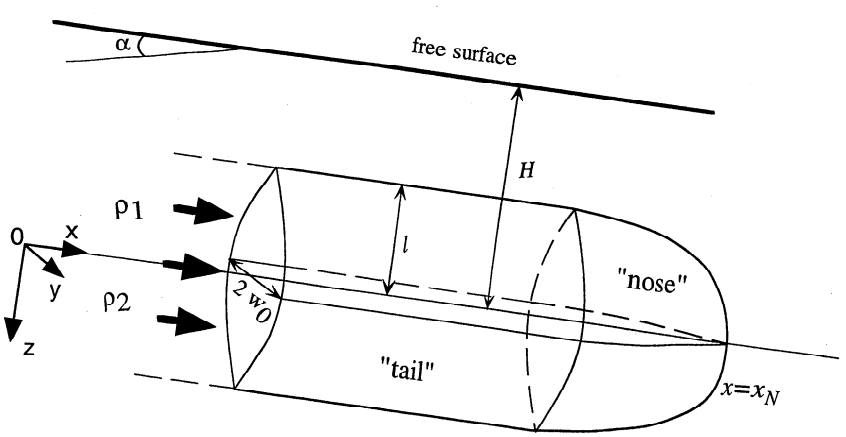

Figure 1. Schematic picture of a dike tracking the level of neutral buoyancy (LNB) in the presence of a small topographic gradient. Far from the nose the excess magma pressure approaches a constant value p. For simplicity we assume that the excess magma pressure in any vertical cross section varies linearly and symmetrically about the dike centerline (x axis in Figure 1). For the density-controlled LNB (i.e., in the absence of any deviatoric tectonic stress) this assumption implies a density contrast between the magma and the host rocks $\Delta\rho=(\rho_2-\rho_1)/2$, where ρ_1 and ρ_2 are the density of the solid above and below the LNB, respectively, and a magma density ρ_m such that $\rho_2>\rho_m>\rho_1$ and $|\rho_1-\rho_m|=\rho_2-\rho_m$. In this case, the dike width is maximum in the horizontal cross section z=0 [e.g., *Lister*, 1990].

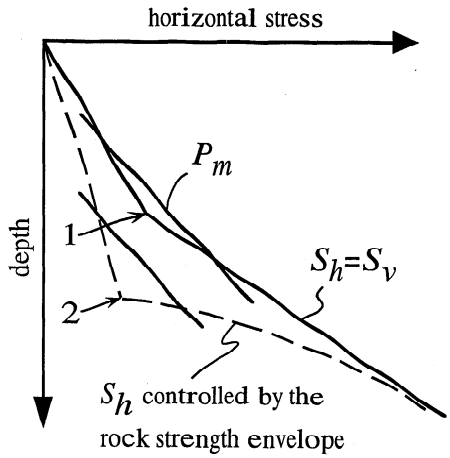

Figure 2. Two distributions of the least horizontal stress S_h capable of giving rise to laterally propagating dikes. For $S_h = S_v$ (solid line), dike is trapped at the level of neutral buoyancy (1). For S_h controlled by the rock strength in a region undergoing amagmatic extension (dashed line), the depth of "effective neutral buoyancy" becomes the brittle-ductile transition (2). The excess magma pressure is given by the difference between the magma pressure (P_m) and S_h curves.

space surface at a constant depth H. We put neutral buoyancy in quotes because the "effective" LNB is actually controlled by the difference between the vertical gradients in the hydrostatic magma pressure (dP_m/dz) and the ambient lithostatic stress (dS_h/dz, see Figure 2). Hereafter by LNB we imply the depth at which the difference $dP_m/dz - dS_h/dz$ changes sign, and by $\Delta\rho$ we imply the effective density contrast between the magma and the host rocks that implicitly includes the effects of the vertical gradients in the regional (tectonic) horizontal stress. Note that compressive stresses are assumed to be positive.

In the lateral dike propagation model of *Lister* [1990] and *Lister and Kerr* [1991], which neglects thermal effects, dike growth is driven by the localized influx of magma at a prescribed rate Qt^{β}, where t is time and β is a numerical coefficient (a constant source pressure boundary condition is obtained by putting $\beta = 1/2$). Magma flow is presumed to be purely horizontal, and the dike height and thickness profile in any vertical cross section are approximated as being due to the distribution of excess magma pressure in that cross section alone. The lateral flow is driven by the drop in excess magma pressure from the source to the downrift nose of the dike. Thus the dike height and thickness decrease toward the nose, and the pressure gradient for magma flow (and hence the dike velocity) decreases as the dike length increases. Both the decrease in thickness and velocity would enhance magma freezing. However, the along-strike slopes of many volcanic rift zones are sufficient to drive dike propagation at velocities close to those observed (e.g., 0.3 m/s for a dike 1.5 m thick and a magma viscosity of 100 Pa s for the 1% slope along the CoAxial segment of the Juan de Fuca ridge), even without along-strike variations in the excess magma pressure. This suggests that models of lateral dike propagation should account for the fact that the dikes are essentially running "downhill".

The importance of topographic slope in driving lateral magma flow in dikes is readily demonstrated. Coupled elastic-hydrodynamic models of fluid-driven fracture indicate that in the absence of gravity, the pressure gradient driving the flow is of the order of the excess pressure at the magma source, $p(0)$, divided by the dike length x_N (Figure 1) [e.g., *Spence and Turcotte*, 1985]. If the LNB maintains a constant depth beneath the surface, the driving pressure gradient due to gravity will be $G = \rho_m g \sin\alpha$ for a subaerial rift and $(\rho_m - \rho_w) g \sin\alpha$ for a submarine rift, where ρ_w is seawater density. Comparing these pressure gradients, we find that the driving pressure gradient due to submarine topography dominates the flow when $x_N > p(0)/[(\rho_m - \rho_w) g \sin\alpha)]$. Taking $p(0)$ = 5 MPa as a typical estimate of the excess pressure at the source (see section 2.1), ρ_m ~2600 kg/m^3, and α~1-3% as characteristic of along-strike slopes along ridge segments [e.g., *Neumann and Forsythe*, 1993, figure 2]), this requires lateral propagation distances of only 10 to 30 km. This is a small fraction of inferred dike propagation distances in Iceland, in Hawaii and on the Juan de Fuca ridge, and it is also less than the half length of many ridge segments along the Mid-Atlantic Ridge (MAR). Thus for long dikes the topographic slope may provide a substantially larger pressure gradient for flow than does the excess source pressure.

Note that for a dike following a topographic slope, gravity can drive the flow while the excess pressure that dilates the dike remains constant. It follows that in the absence of freezing, a dike driven by a constant topographic slope could maintain a constant thickness along any cross section parallel to the x axis (excluding the nose region where the 3-D elasticity effects would narrow the dike aperture over distances of the order of the dike height behind the dike tip). For simplicity, we replace the elastic fissure with a rigid parallel-wall slot of initially constant thickness $2h$ (Figure 3). Thus we neglect the elastic response of the dike walls to modifications in the fluid pressure due to freezing and viscous pressure losses and any variation in dike thickness with depth.

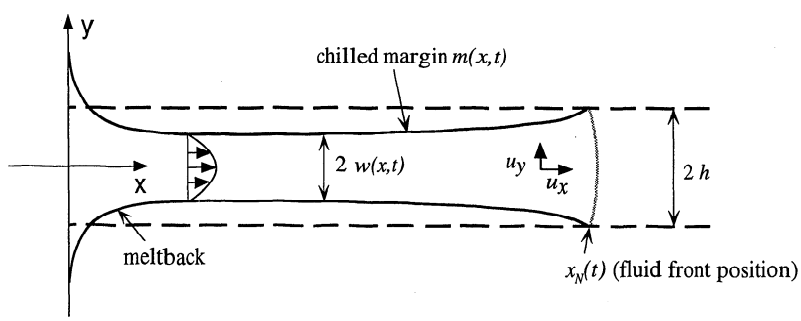

Figure 3. A parallel-wall channel of initial width $2h$ having infinite extent in positive x direction is filled by hot fluid injected at $x = 0$. Geometry of the fluid-occupied portion of the channel is governed by crystallization/melting at the phase boundary.

We treat the flow as being driven by a combination of a drop in excess magma pressure from the source to the fluid front, ΔP, and a pressure gradient due to topography, G. The relevance of this problem to laterally propagating dikes is considered further in section 5. We proceed with the identification of important physical scales relevant to the fluid-mechanical and thermodynamic parts of this problem.

2.1. Pressure Scales and Fluid Dynamics

Since in our model the magma conduit is considered to be rigid-walled, we are interested in values of the excess magma pressure p only insofar as they may allow one to estimate reasonable values of ΔP. For a sufficiently long dike ($x_N >> l$, where l is the dike half height), plain strain conditions will be satisfied in any cross section perpendicular to the x axis except near the dike nose (leading edge, see Figure 1). It follows that given the pressure distribution within any vertical cross-section, the dike shape in that cross-section is governed by two-dimensional elasticity. Given that the excess magma pressure in any vertical cross-section is the sum of the excess pressure at the dike center p and a piecewise linear hydrostatic pressure $\Delta\rho g z\cos\alpha$, where $\Delta\rho$ is negative above the LNB and positive below (Figures 1 and 2), one can find the dike height $2l$ and the maximum dike width $2h$ using analytical solutions for a 2-D elastic crack in an infinite body [e.g., *Lister*, 1990; *Khazan and Fialko*, 1995]:

Dike half height l
$$l=\frac{\pi}{2}\frac{p}{\Delta\rho g\cos\alpha} \tag{1}$$

Dike half thickness h
$$h=\frac{1}{2}\frac{p}{M}l \tag{2}$$

In (2), M is elastic stiffness, $M=\mu/(1-\nu)$, where μ is shear modulus and ν is Poisson's ratio. Estimates (1) and (2) are obtained assuming that the excess pressure distribution is linear and symmetric with respect to the LNB and that the stress intensity factors at the upper and lower crack tips equal zero. A typical width of basaltic dikes in the volcanic rift zones of Iceland and Hawaii as well as in exposed ophiolite complexes is of the order of 1 m [*Gass*, 1989]. Taking M=10 GPa and $\Delta\rho$=300 kg/m^3 as representative values for the oceanic crust [e.g., *Rubin*, 1995], from (1) and (2) we find that a 1 m thick dike should have an excess pressure p of the order of 4 MPa and a (full) height of the order of 4 km.

Estimates of the Reynold's number for the magma flow based on observed dike thicknesses w~O(1 m) and propagation velocities u~O(1 m/s) indicate that for typical values of the dynamic viscosity of basic melts, η ~$O(10^2$ Pa s), magma flow in laterally propagating dikes is laminar and can be analyzed using lubrication theory [e.g., *Bruce and Huppert*, 1990; *Lister and Kerr*, 1991]. The dike is essentially narrow so that the dike walls can be considered as locally parallel. Then the along-stream component of the fluid velocity in any horizontal cross section is given by planar Poiseuille flow

$$u_x=-\frac{1}{2\eta}\left(w^2-y^2\right)\left(\frac{\partial p}{\partial x}-G\right), \qquad (|y|\le w) \tag{3}$$

where $2w$ is the local dike aperture available for flow, $\partial p/\partial x$ is the gradient in excess pressure, and G is the driving pressure gradient due to topography. For the problem shown in Figure 3, $u_z=0$ and the only nonzero cross-stream component of the fluid velocity u_y can be obtained from (3) using the local condition of continuity div u = 0,

$$u_y=\frac{y}{2\eta}\left[\left(w^2-\frac{y^2}{3}\right)\frac{\partial^2 p}{\partial x^2}+2w\frac{\partial w}{\partial x}\left(\frac{\partial p}{\partial x}-G\right)\right] \tag{4}$$

(assuming that dG/dx =0). The fluid-mechanical part of the problem is closed by the equation of mass conservation

$$2\frac{\partial h}{\partial t}=-\frac{\partial q}{\partial x}\ . \tag{5}$$

In (5), h is the mechanical half-opening of the channel and q is the local volumetric flux,

$$q=2w\bar{u}_x=-\frac{2}{3}\frac{w^3}{\eta}\left(\frac{\partial p}{\partial x}-G\right), \tag{6}$$

where $\bar{u}_x$ is the cross-sectionally averaged along-stream velocity. Note that h can be written as a sum of the local channel half aperture w and the thickness of the chilled margin m, $h(x,t)=w(x,t)+m(x,t)$. For the rigid-wall channel, $\partial h/\partial t=0$ and from (5) it follows that at any time the flux q should be constant everywhere along the channel. In this case, combination of (4) and (6) gives rise to the following relation between u_x and u_y:

$$u_y=\frac{y}{w}\frac{\partial w}{\partial x}u_x\ . \tag{7}$$

The total viscous pressure drop available to drive the flow is the sum of that due to the drop in excess pressure ΔP and that due to topography,

$$-\int_0^{x_N}\left(\frac{\partial p}{\partial x}-G\right)dx=\Delta P+Gx_N\ . \tag{8}$$

The local driving pressure gradient is related to the global volumetric flux as $\partial p/\partial x-G=-1.5\eta q/w^3$ (equation (6)); substituting this into (3), (7) and (8), we find that the fluid velocity in the channel may be written as

$$\boldsymbol{u}=\left\{u_x,u_y\right\}=\frac{3}{4}\frac{w^2-y^2}{w^3}q(t)\left\{1,\frac{y}{w}\frac{\partial w}{\partial x}\right\}, \tag{9}$$

where the global volumetric flux $q(t)$ depends on the fluid viscosity, the total pressure drop driving the flow and the channel geometry:

$$q(t)=\frac{2}{3\eta}\frac{\Delta P+Gx_N(t)}{\int_0^{x_N(t)}\frac{dx}{w^3(x,t)}}\ . \tag{10}$$

The channel geometry is governed by the processes of solidification and/or melting concomitant with the magma flow. In essence, the above approach is an extension of the formulation of *Lister and Dellar* [1996] to the case of flow in a semi-infinite channel.

2.2. Heat Transfer

We suppose that the magma and the host rocks are indistinguishable except by phase. This assumption is reasonable for basalts intruding oceanic crust. Typical thermophysical parameters for basalts that will be used

throughout this paper are thermal diffusivity $\kappa=10^{-6}$ m^2 s^{-1}, solidus temperature T_s =1150°C, heat capacity c =1 kJ kg^{-1} °C^{-1} and latent heat of crystallization/fusion L=500 kJ kg^{-1} [e.g., *Rubin*, 1995]. We assume that the magma enters the channel at uniform temperature T_m ($T_m \geq T_s$) and that the initial host rock temperature is T_0. Scaling arguments suggest that the thermal transport problem can be parameterized in terms of two dimensionless numbers [*Bruce and Huppert*, 1990; *Lister*, 1994a], which we choose to be

$$\text{Stefan number} \qquad S=\frac{L}{c(T_m-T_0)} \tag{11}$$

$$\text{Dimensionless solidus temperature} \qquad \Theta=\frac{T_s-T_0}{T_m-T_0} \tag{12}$$

Early studies of the thermal effects of dike propagation [e.g., *Fedotov*, 1978; *Spence and Turcotte*, 1985] were restricted to calculations of the "thermal entry" length, which physically represents the distance at which the incoming fluid has lost essentially all of its heat to the surroundings. It may be calculated as the product of a characteristic solidification time for a stationary fluid and an average velocity of the fluid in the absence of freezing. The estimate of the static solidification time for a parallel-walled channel of thickness $2h$ is given by

$$\tilde{t}=\frac{h^2}{4\lambda^2\kappa}, \tag{13}$$

where h^2/κ is a characteristic diffusion time and $\lambda(S,\Theta)$ is given by [*Carslaw and Jaeger*, 1959]

$$\lambda=\frac{\exp(-\lambda^2)}{\pi^{1/2}S}\left[\frac{\Theta}{\operatorname{erfc}(-\lambda)}-\frac{1-\Theta}{\operatorname{erfc}(\lambda)}\right]. \tag{14}$$

In (14), erfc denotes the complementary error function. Solutions to (14) for a range of parameters S and Θ are shown in Figure 4. The thermal entry length can then be estimated as $\tilde{x}\equiv\bar{u}_x\tilde{t}$, where $\bar{u}_x=h^2\Delta P/3\eta x_N$ for a flow driven by a constant source pressure ΔP and $\bar{u}_x=h^2G/3\eta$ for a flow driven by a constant global pressure gradient G (equation (3)). This yields the following estimates for the thermal entry length:

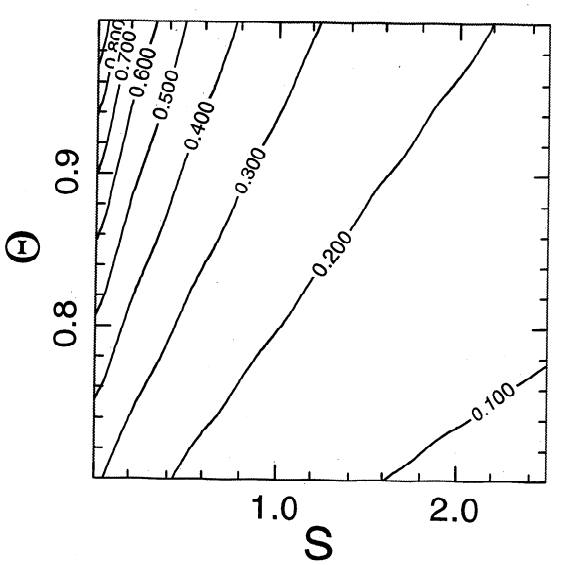

Figure 4. Numerical values of parameter λ satisfying equation (14).

$$\text{Excess pressure-driven} \qquad \tilde{x}=\frac{h^2}{2\lambda}\left(\frac{\Delta P}{3\eta\kappa}\right)^{1/2} \tag{15}$$

$$\text{Topography-driven} \qquad \tilde{x}=\frac{h^4G}{12\lambda^2\eta\kappa}. \tag{16}$$

Because expressions (15)-(16) are the unique lengthscales in this problem, any flow into an infinite rigid-walled channel will eventually freeze, even for an unlimited source, provided that viscous dissipation in the fluid is negligible (see below). Thus this case differs qualitatively from that of flow in a finite channel [*Bruce and Huppert*, 1990; *Lister and Dellar*, 1996], where unlimited meltback of the channel walls is predicted for sufficiently large fluid velocities.

For T_m=1200°C, T_0=0°C, ΔP =5 MPa, $G=(\rho_m-\rho_w)g\sin\alpha$ ~0.3 MPa km^{-1} (a typical driving pressure gradient due to a 2% along-strike slope) and η=100 Pa s, from (15) and (16) we find that a 1 m wide basaltic dike would have a thermal entry length of ~20 km if driven by the excess pressure alone and ~43 km if driven by topography alone. While these numbers are intriguingly close to the observed wavelengths of crustal thickness variations on the MAR, the strong dependence of the thermal entry length on the dike width ($\propto h^2$ and $\propto h^4$ for the end-member cases described by (15) and (16), respectively) suggests that moderate increases in dike thickness could allow dikes to travel distances far exceeding the lengths of ridge segments before freezing. However, estimates (15)-(16) do not account for decreases in the propagation velocity because of channel constrictions due to solidification. This effect has a strong positive feedback since the decreasing fluid velocities decrease the amount of advected heat, which further enhances freezing (the opposite effect is also possible, i.e., when meltback of the channel walls increases the total flux of magma [*Bruce and Huppert*, 1990]). Therefore specifically tailored numerical experiments are required to investigate the flow evolution in space and time.

Consider the thermal evolution of a fluid flowing into a semi-infinite rigid-wall channel (Figure 3). Conservation of energy in the fluid [$0<x<x_N(t)$, $|y|<w(x,t)$] is given by

$$\frac{\partial T}{\partial t}+\boldsymbol{u}\cdot\nabla T=\kappa\nabla^2T, \tag{17}$$

where $T=T(x,y,t)$ is fluid temperature, t is time, and the components of the velocity vector $\boldsymbol{u}$ are given by equation (9). In the solid [$|y|>w(x,t)$], temperature obeys an ordinary diffusion equation

$$\frac{\partial T}{\partial t}=\kappa\nabla^2T. \tag{18}$$

We define a Peclet number Pe as the ratio of the characteristic timescales for diffusion (w^2/κ) and advection ($w/\bar{u}_x$), so that $Pe\sim O(q/\kappa)$, where q is given by (10). Unless the dike is almost completely halted by freezing, the magma flow is characterized by large Peclet numbers, $Pe \gg 1$, which means that along-stream conduction is negligible compared with advective heat transport. In this case, the Laplacians (∇^2T) in (17)-(18) reduce to $\partial^2T/\partial y^2$. The fluid-mechanical and thermal parts of the problem are coupled by the equation governing the rate of chilled margin growth [*Carslaw and Jaeger*, 1959]

$$\rho_m L\frac{\partial m}{\partial t}=-k\left[\frac{\partial T}{\partial y}\right]_-^+. \tag{19}$$

In (19), k is thermal conductivity and brackets denote the jump in temperature gradient across the solid-liquid interface, $[f]_-^+ = f|_{y=w+} - f|_{y=w-}$. For the rigid-walled channel, $w(x,t)+m(x,t)=\text{const}=h$, so that $\partial w/\partial t = -\partial m/\partial t$. At the phase boundary $[|y|=w(x,t)]$ the temperature equals the solidus temperature T_s. The flow ceases when $w=0$ at some point along the channel. Following *Bruce and Huppert* [1990] and *Lister* [1994a], we treat the fluid phase as isoviscous, assuming that the temperature effect on fluid viscosity is dominated by a step increase at $T = T_s$. The full numerical solution to this problem is presented in section 3.

In general, fluid superheat and latent heat of crystallization are not the only sources of energy that may impede freezing. Fluid flow is a dissipative process in which viscous pressure losses are ultimately transformed into heat. The significance of viscous heating compared with the other sources of heat energy in the fluid is characterized by the Brinkman number, which represents the ratio of the viscous heat generation to conductive heat loss [e.g., *Delaney*, 1987; *Rubin*, 1995]

$$Br = \frac{h^4 G^2}{\eta k (T_m - T_0)} \tag{20}$$

(for the topography-driven flow). Using the same parameters as in the calculation of the thermal entry length (equation (16)), from (20) one may conclude that viscous dissipation should not be important in dikes that are thinner than ~2 m (for a 2 m wide dike, Br ~ 0.3). Judging by ophiolite observations, this condition is satisfied for the majority of mid-ocean ridge dikes [e.g., *Gass*, 1989; *MacLeod and Rothery*, 1992], and therefore we will neglect viscous dissipation in most of our simulations. It should be mentioned, however, that the strong dependence of viscous heating on the channel width ($\propto h^4$) and driving pressure gradient ($\propto G^2$) indicates that Brinkman numbers of order unity might be reached by some large dikes, which thus would be able to propagate as long as the available driving pressure gradient does not drop below some critical value (for example, when the topographic slope levels off). Note that when the conductive heat loss is balanced or exceeded by viscous dissipation, the dike would be able to propagate downrift even when the source becomes depleted and the supply of new magma decreases.

3. Scaled System of Equations and Numerical Solution

This section gives the mathematical details of our simulations. Readers who are not interested in these details may proceed directly to section 4.

We consider two cases of flow in a rigid parallel-walled channel of infinite extent. In case 1, the flow is driven by the source excess pressure ΔP only, and in case 2 it is driven by a combination of the source pressure ΔP and a constant global (e.g., topographic) pressure gradient G. We define dimensionless temperature θ,

$$\theta = (T - T_0)/(T_m - T_0), \tag{21}$$

as suggested by (11). Dimensional analysis of (9)-(10) and (17)-(18) prompts the following scalings for variables x, y, and t:

$$\text{Case 1} \qquad \hat{x} = h^2\left(\frac{\Delta P}{\kappa\eta}\right)^{1/2},$$

$$\text{Case 2} \qquad \hat{x} = h^4\frac{G}{\kappa\eta}, \tag{22}$$

$$\hat{y} = h, \quad \hat{t} = \frac{h^2}{\kappa}.$$

Expressions (22) in turn imply the following dimensional scales for the fluid velocities:

$$\text{Case 1} \qquad \hat{u}_x = \left(\frac{\Delta P \kappa}{\eta}\right)^{1/2},$$

$$\text{Case 2} \qquad \hat{u}_x = \frac{h^2}{\eta}G, \tag{23}$$

$$\hat{u}_y = \frac{\kappa}{h}.$$

Nondimensionalization of (17)-(18) and (9)-(10) using (22)-(23) gives rise to the following system of equations:

$$\frac{\partial\theta}{\partial t} + \frac{1}{2}\frac{w^2 - y^2}{w^3}F(t)\left(\frac{\partial\theta}{\partial x} + \frac{y}{w}\frac{\partial w}{\partial x}\frac{\partial\theta}{\partial y}\right) = \frac{\partial^2\theta}{\partial y^2} \quad (|y|<w), \tag{24}$$

$$\frac{\partial\theta}{\partial t} = \frac{\partial^2\theta}{\partial y^2} \qquad |y|>w, \tag{25}$$

for $0 < x < x_N(t)$. In (24), $F(t)$ is a modified dimensionless flux,

$$\text{Case 1} \qquad F(t) = \left(\int_0^{x_N}\frac{dx}{w^3}\right)^{-1},$$

$$\text{Case 2} \qquad F(t) = \frac{\Gamma + x_N}{\int_0^{x_N}\frac{dx}{w^3}}, \quad \Gamma = \frac{\Delta P \kappa\eta}{h^4 G^2}, \tag{26}$$

where the parameter Γ is essentially a ratio of the driving pressure gradients due to the excess source pressure and due to topography. Equation (19) coupling the growth of the chilled margin with the temperature field may be written as

$$\frac{\partial w}{\partial t} = \frac{1}{S}\left[\frac{\partial\theta}{\partial y}\right]_-^+ \qquad (|y|=w). \tag{27}$$

Equations (24) and (25) are subject to the following initial and boundary conditions:

At $t = 0$,

$$w=1 \text{ for } 0<x<\infty; \qquad x_N << 1; \qquad \theta = 0 \text{ for } |y|>1. \tag{28}$$

For $t \geq 0$,

Incoming fluid temperature

$$\theta = 1 \text{ for x=0 and } |y| < w(0,t). \tag{29}$$

Phase boundary is at the solidus temperature

$$\theta = \Theta \text{ for } |y| = w. \tag{30}$$

Chill thickness is zero at the fluid front

$$w=1 \text{ for } x=x_N. \tag{31}$$

Temperature at infinity

$$\theta = 0 \text{ for } |y| \to \infty. \quad (32)$$

The Stefan number S and nondimensional solidus temperature Θ were defined by (11) and (12), correspondingly.

It should be mentioned that (24) is hyperbolic in x and t, and thus the "upstream" temperature boundary condition should be specified at $x=x_N$. *Lister* [1994a] proposed that the appropriate boundary condition at the fluid front is "temperature turn-around", in which the temperatures of the incoming streamlines (in the reference frame of the moving front) are identified with the temperatures on the corresponding outgoing streamlines (see *Lister* [1994a] for details). The flow near the fluid front (closer than several channel thicknesses) becomes essentially two-dimensional and the simple parabolic velocity profile given by (3) cannot be assumed. The details of the advection there may be neglected as long as $Pe \gg 1$, but the upstream boundary condition should reflect the fact that the fast moving fluid in the center of the channel is placed against the cold walls at the moving fluid front. In our calculations, we assumed that the temperature at the fluid front is an average of the temperatures associated with the incoming volume of fluid during the current time step. We found that different energy-conserving upstream boundary conditions have little effect on the global flow evolution.

Details of a numerical solution of the system (24)-(27) are given in the appendix. It should be mentioned that the incompatible temperature boundary condition at the point (0, w) requires simultaneously $\theta=1$ and $\theta=\Theta$ and thus an infinite rate of meltback at all times (unless $\Theta=1$, i.e. if the fluid is injected at the solidus temperature). Therefore the channel thickness at $x=0$ is ill-defined. In particular, $w(0, t)$ intrinsically depends on the cross-stream mesh discretization because the latter controls the temperature gradient in the fluid ($\partial\theta/\partial y|_{x=0,y=w-} = (1-\Theta)/\Delta y$, where Δy is grid spacing). Trials with different mesh sizes and time steps show that this incompatibility (apparently also present in the model of *Lister and Dellar* [1996]) does not affect the accuracy of calculations more than two grid points downstream.

4. Results

Figure 5 shows the evolution of the temperature field and channel geometry for a flow driven by a constant global pressure gradient alone (case 2, $\Gamma = 0$) for S=0.5 and Θ=0.9 (e.g., corresponding to T_m=1250°C and T_0=250°C). At early times, solidification proceeds everywhere along the channel wall. Because the temperature gradients are large, heat conduction dominates advection. For this reason, and because the propagation velocity is nearly constant, the chilled margin acquires a characteristic parabolic profile beyond the fluid front. Two thermal boundary layers are formed in the fluid: one associated with conductive cooling of the incoming hot fluid along the channel wall, and another due to temperature turn-around at the fluid front. At later times, the continual supply of heat stops freezing near the source and reverses the migration of the phase boundary, causing meltback of the initial chill and, subsequently, of the original solid. As mentioned above, for numerical reasons the channel thickness at $x = 0$ is ill-defined. Eventually, the fluid loses its superheat through conduction to the host solid and quickly solidifies thereafter (Figure 5c). Progression of the fluid front in time is shown in Figure 6a. Figure 6b shows the migration of earthquakes associated with the July 1978 dike intrusion north of the Krafla caldera, Iceland [*Einarsson and Brandsdottir*, 1980], which propagated down a slope of ~1%. Although lateral gradients in the ambient horizontal stress might also play a role in driving the magma flow, the qualitative similarity between Figures 6a and 6b suggests that the decrease in migration velocity might manifest thermal arrest at ~30 km from the source (center of the caldera).

For dikes intruding oceanic crust, the initial magma temperature T_m may vary from the solidus (~1150°C) to

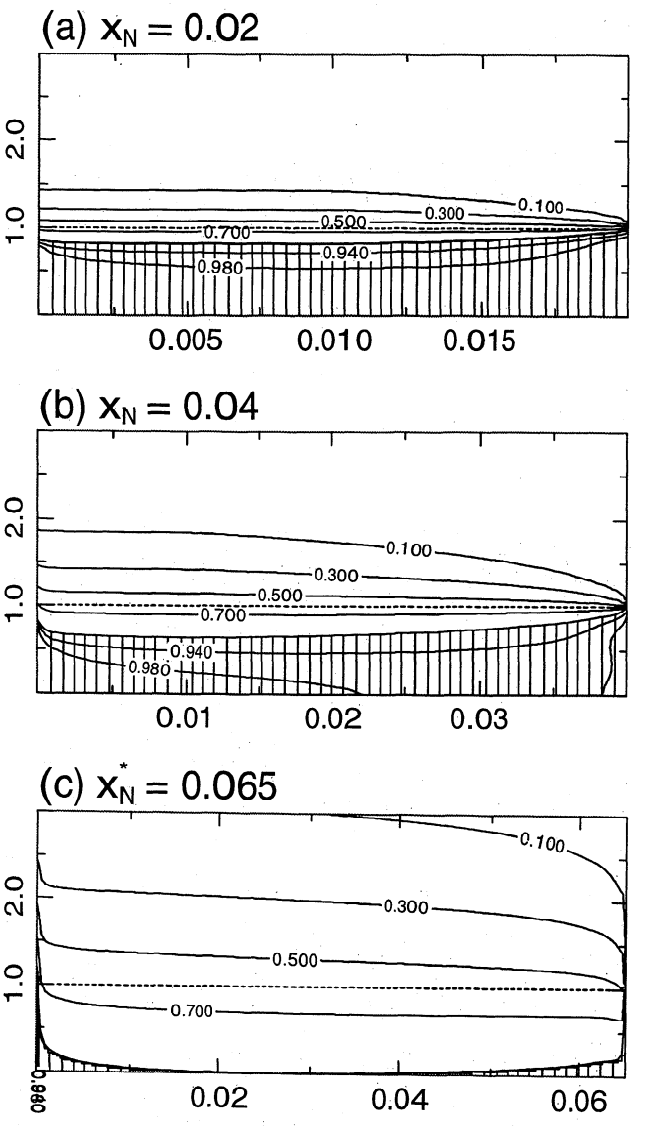

Figure 5. Development of the temperature field and channel geometry for a flow driven by a constant driving pressure gradient (case 2, $\Gamma = 0$) for S = 0.5 and Θ = 0.9. Vertical axis is scaled in units of the initial channel thickness (dotted line) and horizontal axis is normalized by the current nondimensional distance from the source to the magma front $x_N(t)$. Chilled margin (solid line following the 0.9 isotherm) grows inward as the fluid loses its heat due to conductive cooling. Fluid region is hatched; x_N^* is nondimensional thermal arrest length (see equations (22)).

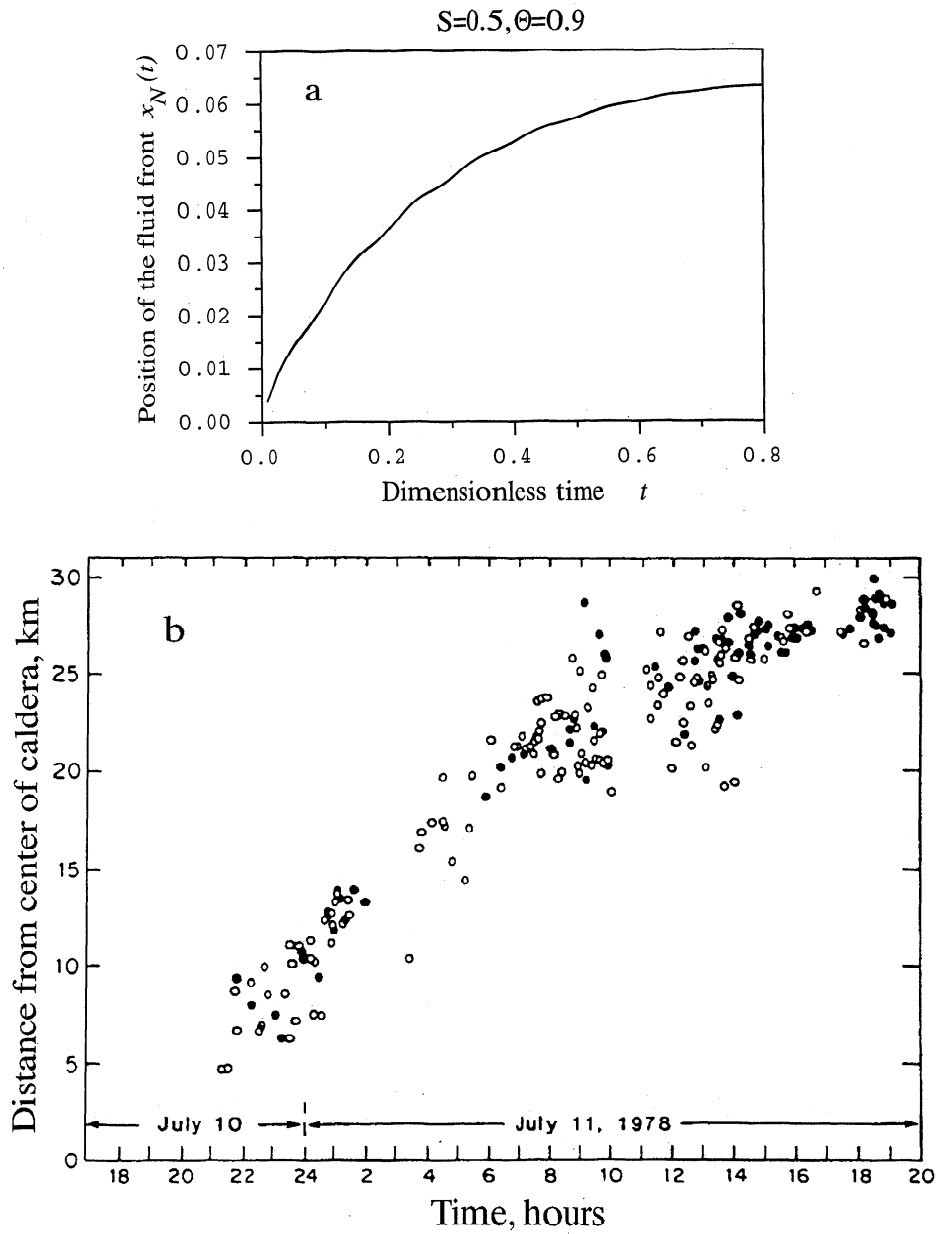

Figure 6. (a) Dimensionless position of the fluid front as a function of dimensionless time for the problem shown in Figure 5. Time derivative of the fluid front position gives the propagation velocity and the volumetric flux in the channel as a function of time. (b) Migration of seismic activity along the fissure swarm north of the Krafla caldera during the July 1978 dike intrusion. From *Einarsson and Brandsdottir* [1980], reproduced with permission of the Springer Inc.

perhaps 1300°C. Although the initial temperature of the host rocks T_0 may in principle approach the solidus, the dike thickness is expected to decrease below the brittle-ductile transition because of the increase in horizontal compressive stress (Figure 2). Because increases in thickness will be seen to be much more significant than increases in temperature, we limit the range of the initial host rock temperature from 0°C to some 600°C. According to (11)-(12), this limits the range of the Stefan number to $0.4 < S < 2$ and the dimensionless solidification temperature to $0.75 < \Theta \le 1$. The parameter Γ, defined by (24), may vary widely (for reasonable geophysical parameters, $\Gamma < 1$; note that for $\Gamma >> x_N^*$, case 1 is recovered). Figure 7a shows dimensionless solidification distances x_N^* for flows driven by a fixed pressure drop between the magma source and the magma front (case 1) for a range of geologically reasonable values of S and Θ. Figure 7b shows analogous results for case 2 for $\Gamma = 0$ and $\Gamma = 0.17$ ($\Gamma = 0.17$ corresponds, for example, to a 1.5 m wide dike driven by an excess source pressure of 5 MPa and an along-strike topographic gradient of 0.3 MPa km^{-1}). These thermal arrest distances can be made dimensional using scalings (22) (see section 5).

4.1. Effect of a Narrow Dike Tip

Solutions from section 3 would be directly applicable to lateral dike propagation if magma was traveling through an open fissure of fixed width. In reality, dikes propagate via elastically widening existing or self-induced fractures in the host rock. One consequence of this for laterally propagating

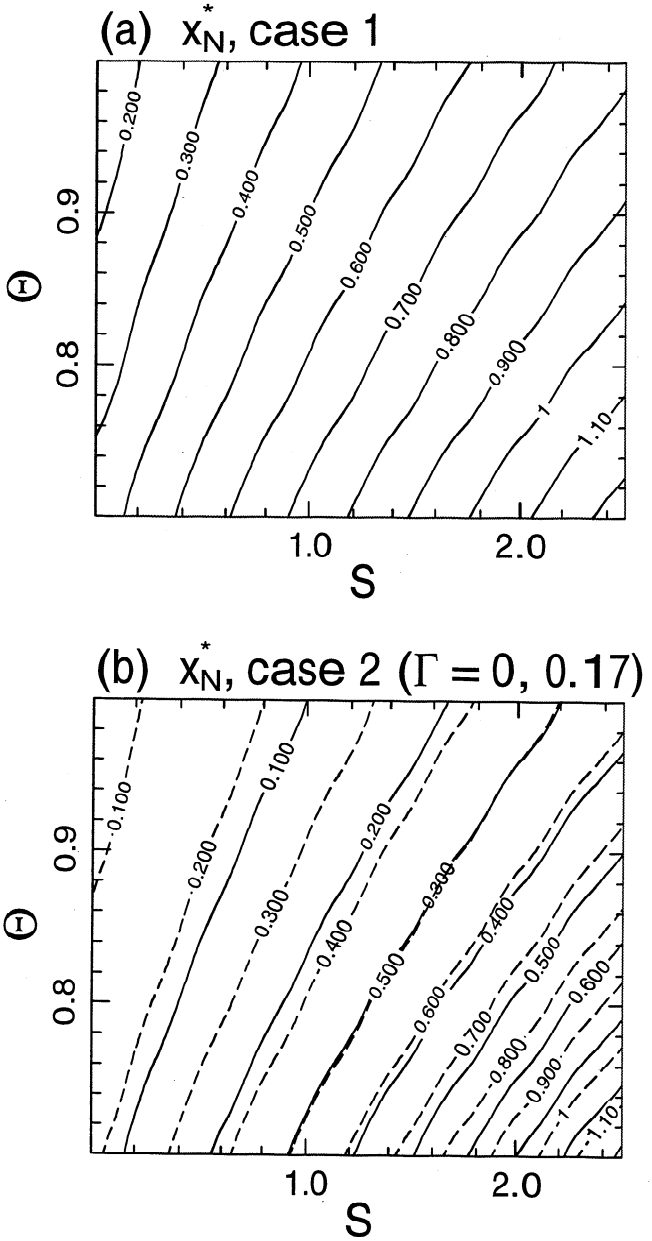

Figure 7. Dimensionless thermal arrest distances x_N^* calculated for geophysically relevant range of parameters S and Θ for a flow driven by (a) fixed pressure drop from the source to the fluid front, and (b) constant global (e.g., topographic) pressure gradient (solid contours) and a combination of a fixed pressure drop and a constant global pressure gradient ($\Gamma = 0.17$, dashed contours).

dikes is that elasticity narrows the channel behind the dike tip over distances of the order of the dike height (i.e., within the "nose" region in Figure 1). There are several reasons to suspect that the narrow dike nose may affect the overall propagation. First, the magma in the nose is most susceptible to freezing because it has cooled the most and because it comes in contact with the coldest rocks. Second, the mechanical narrowing of the dike walls provides the opportunity for the rapidly growing chilled margin to block the flow. Given a nearly constant propagation velocity, the chilled margin grows approximately as the square root of distance behind the magma front. The shape of the elastic crack depends on the pressure distribution within the crack, and the crack profile behind the fluid front may widen more slowly than the square root of distance, especially near the magma front [e.g., *Rubin*, 1993a, Figure 3]. Thus, in the nose region there is a competition between the rate of the elastic widening of the dike and the rate of chilled margin growth. Depending on which rate is larger, the nose will either entirely freeze or propagate in some quasi steady state fashion. Hence it is of interest to quantify the effect of the dike nose on the global flow evolution.

Because our model of the magma flow in the dike "tail" (Figures 1 and 3) does not explicitly include elasticity, we use an ad hoc approach and combine solutions for the rigid channel with solutions for the steadily moving nose of the prescribed shape (see the appendix for details). Figure 8 shows the results of the coupled simulation for the problem

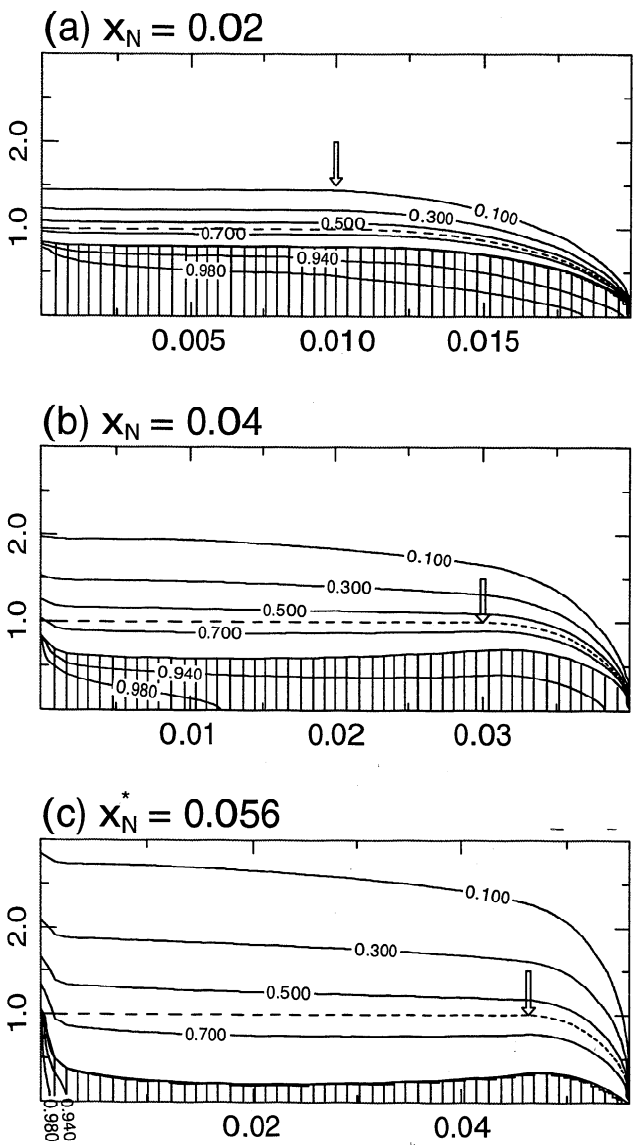

Figure 8. Combined rigid-wall channel - rigid nose solutions for the same model parameters as in Figure 5. Arrows mark junction between the "nose" and the "tail" (see section 4.1. for details). Other notation is the same as in Figure 5.

shown in Figure 5 and for a dimensionless nose length of 10^{-2} (corresponding to a dike that is 4 km tall and ~1 m wide, see equations (1), (2) and (22)) and a thickness at the magma front that is 10^{-2} times that in the tail (the majority of exposed dikes in Iceland have thicknesses at the magma front of the order of several centimeters [e.g., *Gudmundsson*, 1995]). The flow becomes constricted first at the tip of the nose when the propagation velocity drops to about several percent of the prefreezing value (which is the steady state value for topography-driven flows). Such behavior is confirmed by fully coupled elastic - fluid-mechanical - thermodynamic simulations of the dike nose propagating at constant speed; in these calculations the magma was assumed to enter the nose at solidus temperature (unpublished results). Note that the reduction in the propagation velocity is primarily due to solidification in the dike tail (the appendix). The calculated thermal arrest distance is ~ 20% shorter than the analogous nose-absent solution (Figure 5). Note that the dimensionless nose length decreases dramatically with modest increases in the (dimensional) dike thickness; this is because the thermal entry length increases as the fourth power of the dike thickness (equation (22)), while the dimensional nose length (constrained by the dike height) increases only as the square root of thickness (equations (1) and (2)). For noses that have smaller nondimensional length, the overall effect on the global flow evolution is less.

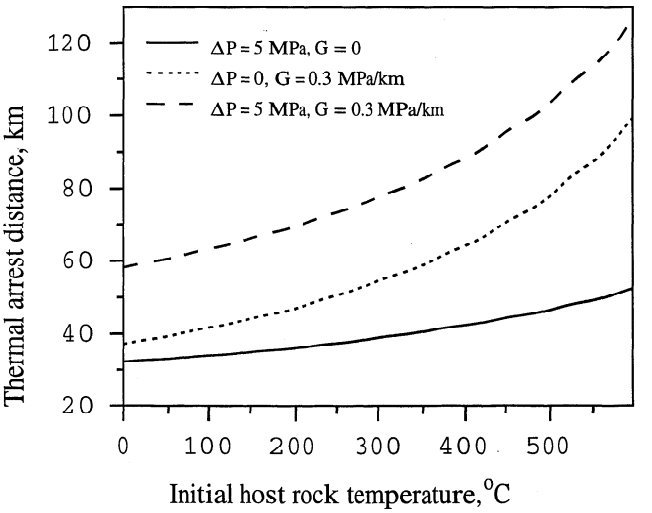

Figure 9. Maximum distance basic magma may travel through a 1.5-m-wide slot before the channel is constricted by freezing, as a function of the initial solid temperature (data taken from Figure 7). (1) Solid line is for a flow driven by a constant pressure drop of 5 MPa along the channel; (2) dotted line is for a flow driven by a constant global pressure gradient of 0.3 MPa/km (corresponding to a submarine slope of 2%); (3) dashed line is for a flow driven by a combination of 1 and 2. Initial magma temperature is assumed to be 1200°C, solidus temperature is 1150°C, thermal diffusivity is 10^{-6} m^2 s^{-1}, latent heat of fusion is 500 kJ kg^{-1} and heat capacity is 1 kJ kg^{-1} °C^{-1}.

5. Discussion

The computed thermal arrest distances (Figure 7) can be made dimensional using scalings (22), and the thermal parameters can be retrieved from (11)-(12) given particular values of the Stefan number S and dimensionless solidification temperature Θ. Figure 9 shows dimensional results for several examples. In the first example (solid line in Figure 9), the flow is driven by a fixed pressure drop of 5 MPa from the source to the magma front. In the second example (dotted line) the flow is driven by a constant global pressure gradient of 0.3 MPa km^{-1} (corresponding to a submarine topographic slope of 2%), and in the third example (dashed line) by a combination of the fixed pressure drop of the first example and the global pressure gradient of the second example. In all cases, the dike (full) thickness was taken to be 1.5 m (on the high side by ophiolite standards) and the magma viscosity was taken to be 100 Pa s (consistent with measurements in Hawaii). For these parameters, the propagation distance in cold rock is 30 to 40 km for the first two examples (notice that the driving pressure gradient due to gravity becomes dominant when the dike is ~17 km long) and about 60 km for the combined driving pressure gradients. We reiterate that the thermal arrest distances calculated for case 1 more strongly overestimate the distances that dikes may travel than in the analogous calculations for case 2, because for dikes driven by the excess source pressure alone, the mechanical thickness decreases toward the dike nose proportionally to the viscous pressure drop in the magma [e.g., *Lister and Kerr*, 1991].

The scalings (20) indicate that for the topography-driven dike, reducing the thickness by a factor of 2 decreases the propagation distance by a factor of 16; decreasing the magma viscosity or increasing the topographic slope by a factor of 2 doubles the propagation distance, etc. Bearing in mind that these calculations with a constant thickness slot all the way to the magma front and an unlimited source volume place an upper bound on thermally admissible dike lengths (provided that viscous dissipation is negligible), it is apparent that freezing can limit the range of most dikes to less than typical segment half lengths along slow spreading ridges (~40 km [e.g., *Schouten et al.*., 1985; *Lin and Phipps Morgan*, 1992]). Several calculations with the viscous dissipation term have been performed; the results demonstrate that shear heating increases the propagation distance for the 1.5 m wide dikes shown in Figure 9 by less than 15%. Factors that might reduce these propagation distances, other than variations in the parameters entering the scaling relations, include the following:

1. The magma source is depleted before the dike is substantially slowed by freezing. Note that the lateral emplacement of ~30 km long dike requires release of ~ 0.1 km^3 of basaltic melt in a single intrusive event; such a volume may be large taking into account typical rates of magma production and a lack of permanent magma chambers at the slow spreading centers [e.g., *Dick*, 1989; *Cannat*, 1996].

2. Results obtained using a rigid-wall channel model are upper bound estimates in that they neglect the decrease in thickness towards the dike top and bottom. For a lateral dike trapped at the LNB, the average dike thickness is about 2 times less than the maximum dike thickness [*Lister*, 1990]. This implies that much of the magma flowing down the "median" (maximum width) cross section is diverted to supply the thinner (more slowly flowing) regions above and below and does not contribute to advancing the magma front; for this reason the dike does not travel as far before being halted by freezing.

3. Large-scale inelastic deformation of the host rocks

associated with dike propagation. Inelastic deformation of the ambient solid is usually neglected in fluid-mechanical models of dike growth, on the assumption that rock fracture resistance is negligible compared with viscous pressure losses in the fluid [e.g., *Lister and Kerr*, 1991]. However, this assumption is questionable if the region of inelastic deformation (the "process zone" at the dike tip) depends on the dike size and/or on the ambient stress field. Scaling of the process zone size with dike length is suggested by field data and theoretical considerations [*Rubin*, 1993b], and the possibility of substantial increases in the rock fracture energy under in situ conditions has been inferred from laboratory experiments [*Fialko and Rubin*, 1997]. Note that large-scale normal faulting induced by lateral dike intrusions is common in regions with preexisting tectonic extension [e.g., *Rubin*, 1992].

As was mentioned above, the average dike thickness is quite sensitive to the excess magma pressure. Given some statistical distribution of excess pressures (which must depend in part upon the strength of the magma reservoir envelope), freezing will tend to restrict thinner dikes to lesser propagation distances. This presumably leads to the observed decrease in dike number and increase in dike thickness with increasing distance from the shallow magma source in eroded rift zones in the British Tertiary Province, Hawaii, and Iceland [e.g., *Speight et al.*, 1982; *Walker*, 1987; *Gudmundsson*, 1990; *Walker et al.*, 1995]. Small variations in the excess magma pressure p could cause dikes to propagate only some 20-30 km on the MAR but up to 100 km in Iceland and Hawaii. For dikes propagating along the LNB due to a density step, the dike thickness depends on the excess magma pressure squared (see equations (1) and (2)), so that the thermal arrest length scales as p^8 for dikes driven by a topographic slope and as p^4 for dikes driven by an excess source pressure. Consequently, a factor of 5 increase in the dike propagation distance may be caused by as little as a 20% increase in the excess pressure at the magma source. Given that magma supply rates are presumably much higher in Iceland and Hawaii and on the Juan de Fuca Ridge than on slow spreading centers on the MAR, a substantial difference in dike propagation distance between these locations is possible. Note that variability in the average dike propagation distance due to variations in the crustal thermal regime alone is much less significant (Figure 9).

Less frequent intrusions beyond the average thermal arrest distance could lead to the increased tendency for "tectonic" as opposed to "magmatic" extension with distance from volcanic centers along the MAR [*Karson et al.*, 1987], as extension in the absence of intrusion leads to the development of stress fields appropriate for normal faulting [e.g., *Rubin*, 1990; *Parsons and Thompson*, 1991]. In a magma-starved region undergoing extension, the depth of effective neutral buoyancy corresponds to the brittle-ductile transition [*Rubin*, 1990, 1995] (see also Figure 2). If the brittle-ductile transition resides within the mantle, then dikes will tend to spread laterally at this depth (whether they are derived laterally from the segment high or vertically from the mantle below). Thus the total melt delivery to the distal ends of ridge segments may be considerably larger than that inferred from crustal thickness alone (although seismic velocities probably rule out more than 25% gabbro in the mantle within a few kilometers of the Moho [*Cannat*, 1996]). At the same time, this would imply that dikes that spread at the deepening rheologically controlled LNB are less likely to erupt. Since volcanics do comprise a significant portion of the supracrustal rocks at the distal ends of many MOR segments [e.g., *Dick*, 1989], this may suggest that beyond the average thermal arrest length the crust might be accreted due to either episodic magma pulses from the underlying asthenosphere, such that the extensional stress field is temporarily reset by the dike intrusions, or to "unusually" large lateral dikes.

If substantial melt fractionation occurs in laterally propagating dikes, our model could explain observed correlations of the magnesium number Mg # (defined as a ratio $Mg/(Mg+Fe^{2+})$) with the along-axis bathymetry [*Hekinian et al.*, 1976; *Thompson et al.*, 1989; *Langmuir et al.*, 1992]. Observed drops in Mg # imply at least 50 to 60% fractional crystallization [e.g., *Bloomer et al.*, 1989], which might be possible in a dike provided freezing is efficient in removing crystals from the melt into the chilled margin (e.g., see Figure 8). If so, and if dikes that are most likely to erupt are statistically "large" ones (i.e., the ones whose thermal arrest length is comparable to the ridge segment length), then basalts that erupt far from the magma supply center would tend to be more fractionated than those that erupt near the center. The data of *Batiza et al.* [1988] show decreasing Mg # over distances of ~25 km, and elevation drops of ~1.5 km, from the axial high along the MAR at 26°S. Beyond this distance the along-axis slope decreases to zero or reverses and Mg # increases; perhaps the break in topographic slope marks the transition from laterally derived basalts to those derived primarily from below. This would be consistent with the occurrence of relatively high-temperature (high Mg #) magmas in the vicinity of the fracture zones. That is, in order to reach the surface, the melt from a hypothetical magma pocket beneath a segment end has to transverse perhaps less than 10 km of the overlying lithosphere, compared with 20-40 km of cold crustal rocks for magmas intruded laterally from a central magma chamber.

Our results also suggest that crustal contamination of primitive melts intruded along the ridge axis from the central magma chamber should be negligible. This stems from the fact that the region of the host rock melting is restricted to less than 1% of the total dike volume for the parameter space

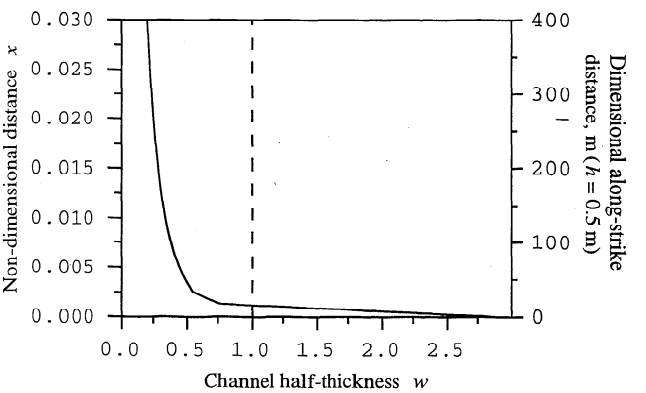

Figure 10a. Detailed picture of near-source thermal erosion for the problem shown in Figure 5c. The exemplary dimensional scale given on the right axis corresponds to an initial channel thickness of 1 m (h=0.5 m), magma viscosity η=100 Pa s, thermal diffusivity $\kappa=10^{-6}$ m^2 s^{-1}, and driving pressure gradient G=300 Pa m^{-1}. Dashed line denotes the initial geometry of the conduit.

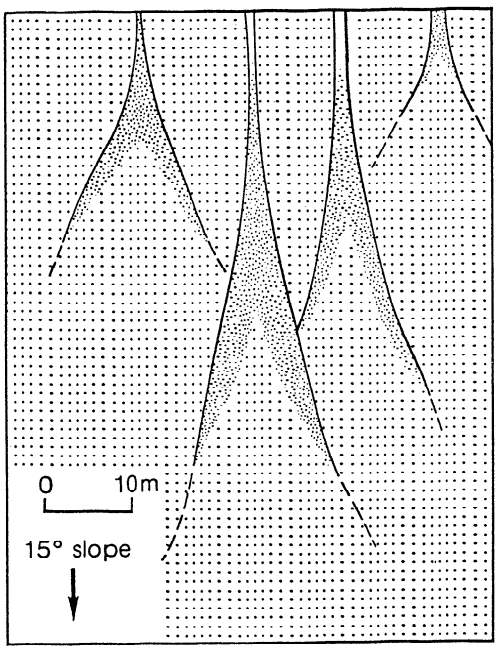

Figure 10b. Field observations of possible meltback of dike walls near the magma source in the Oman ophiolite. Solid lines represent chilled margins, coarse stipple denotes gabbro, and fine stipple denotes microgabbro. From *MacLeod and Rothery* [1992], reproduced with permission of the Geological Society Publication Office.

explored. For the case shown in Figure 5, the meltback is restricted to the very source (cross section x=0) only, even with a mesh of ~800 points along the dike (which corresponds to approximately every 20 m for a dike that is 1 m wide; see Figure 10a). Note that 1-m-wide dikes driven by a pressure gradient of 2 MPa/km would thermally erode the ambient solid indefinitely (or until the source is depleted) in the 2-km finite-channel model of *Lister and Dellar* [1996]. A major difference between the finite and infinite channel models is that when meltback of the initial chilled margin has begun to occur all along the finite channel (at which time meltback of the host rock is restricted to very near the source), the flow in the infinite channel has already solidified at greater distances from the source. Nonetheless, near-source meltback is a very appealing mechanism for producing the inferred widening of some dikes (from about 1 m to perhaps 10 m) as they merge with gabbroic source rocks in the Oman ophiolite (Figure 10b). This gradation occurs over a distance of only a few tens of meters, which is at the limit of our current along-strike resolution (Figure 10a); however, quantitative similarity should not be expected at this stage because of the overall simplicity of the assumed initial conditions (e.g., the solid temperatures near the source are likely to be close to the solidus) and the incompatible boundary conditions at the node corresponding to the source.

As a note for future improvements, the model can be made more realistic by introducing elasticity so that the local channel thickness is coupled to the local pressure. First, this would allow one to determine the fate of a finite batch of magma intruded along the ridge by having the dike thin in response to a pressure decrease. Second, one could compute, rather than stipulate, what the final dike thickness will be (although the dike thickness is controlled by the excess magma pressure through elasticity, ultimately that excess pressure is determined by the interaction of magma flow and freezing as well as the source conditions). By considering the time evolution of the magma pressure uprift of the dike "freezing point" (i.e., the point along the dike where it is first blocked due to solidification), it will be possible to address the question of how freezing influences where the dike might erupt. Finally, by imposing a constant far-field stressing rate, a stress threshold for normal faulting, and a constant or varying magma supply rate, one could systematically examine the nature of the along-strike variation in the ratio of tectonic to magmatic extension. For active ridges where this variation can be inferred from detailed bathymetry, the model results might lead to constraints on typical volumes of injected magma in discrete "spreading" events.

6. Conclusions

We have considered the thermal and fluid-mechanical aspects of lateral dike propagation by simulating the flow of magma into an initially empty channel of constant thickness and unlimited length. Our numerical algorithm accurately accounts for (1) downstream advection of heat in the flowing magma, (2) cross-stream conduction of heat in the magma and host rock, (3) cross-stream advection of heat in the magma (due to downstream variations in the thickness of the frozen margin), and (4) release or absorption of latent heat at the (moving) frozen margin of the dike. Although important aspects of lateral dike growth such as elasticity are not yet included, the rigid-walled channel is an instructive case to consider because it provides an upper bound on the distance that magma may travel, given that viscous dissipation can be neglected for the majority of the MOR dikes. Our results show that for reasonable parameters this upper bound does not exceed the wavelength of crustal thickness variations or transform fault spacing along slow spreading mid-ocean ridges, which indicates that thermal controls on the crustal melt delivery system could be an important factor in modulating these variations.

Along-axis variations in stress are likely to be produced by variations in the ratio of total extension to dike-accommodated extension. For ridges where the spreading rate is uniform and magma is supplied primarily to a central high, as may be the case along much of the MAR [*Schouten et al.*, 1985; *Lin et al.*, 1990], this ratio is most likely determined by the ability of magma freezing to limit the distance that laterally propagating dikes may travel. Magma freezing is also likely to be responsible for larger numbers of thin dikes near the magmatic center and fewer but thicker dikes farther from the center, observed in eroded rift zones in Iceland and the British Tertiary Province.

Appendix: Numerical Scheme Used for Simulation of Freezing of Fluid Flow in a Flat Semi-infinite Channel

The system (24)-(27) together with the boundary conditions (29)-(32) was solved numerically using finite difference techniques. For computational purposes, it is convenient to map the flow region onto a fixed rectangular grid. Correspondingly, we use coordinate transformations

$\bar{y} = y/w(x,t)$ for $|y| < w$, $|\bar{y}| = y - w(x,t) + 1$ for $|y| > w$, and $\bar{x} = x/x_N(t)$. Because of the symmetry about the x axis, the computational domain was restricted to $\bar{y} \geq 0$ and a zero heat flux boundary condition was prescribed across the interval $0 < \bar{x} < 1$, $\bar{y} = 0$. All $\bar{y}$ derivatives were discretized using a Crank-Nicholson scheme. Along-stream derivatives were discretized using second-order upwind differences, except at the grid points adjacent to $\bar{x} = 0$ and 1, where FTCS discretization was used [*Press et al.*, 1992]. The velocity of the fluid front was evaluated based on the volumetric flux at the beginning of a time step, $\dot{x}_N = F(t)/3$. This expression takes into account that $w(1, t)=1$ (boundary condition (31)). Other nonlinear coefficients were estimated at the middle of a time step to obtain a scheme that was second order both in space and time. Time steps were taken to be one-fourth of those allowed by the Courant condition. Integrals in (26) were calculated using Simpson quadrature. Inversion of the system of linear algebraic equations required by the Crank-Nicholson (semi-implicit) discretization admits a tridiagonal structure of the coefficients matrix and can be performed very effectively using a Thompson algorithm.

An adjustable time-dependent grid was used in the solid domain ($\bar{y} > 1$); new points were added to the grid in the $\bar{y}$ direction when the temperature gradient at the "distant" end of the grid (placed initially at $\bar{y} = 3$) exceeded 10^{-3} for a given $\bar{x}$ coordinate. Thus the mesh expanded into the solid together with the thermal boundary layer; when a particular mesh line doubled in length, every other node along this line was tossed out to keep the number of the nodes reasonably low (by the time diffusion proceeds that far into the solid, the temperature profile near the solid-liquid interface becomes essentially linear, and an increase in grid spacing in the $\bar{y}$ direction does not significantly degrade the accuracy of the temperature gradient calculations at $\bar{y} = 1$). A typical calculation (e.g., the one shown in Figure 5) was performed using a mesh of ~170x130 grid points and took about 10^3-10^4 time steps. The accuracy of the code was checked by conservation of energy, by mesh and time step refinements, and by comparison with few available asymptotic solutions. For example, the temperatures associated with the constant velocity flow through a flat duct with isothermal walls and no solidification (Graetz problem) were calculated analytically using eigenfunction expansions [e.g., *Brown*, 1960] and numerically using our code. In this simulation, we assumed very large S (so that the chilled margin growth is negligible), $\Theta = 0$ (no conduction of heat into the solid) and carried calculations until the steady state temperature distribution was reached. The numerical solution converged to the analytical one with an accuracy of the order of the truncation error in the eigenvalue series expansion [*Brown*, 1960].

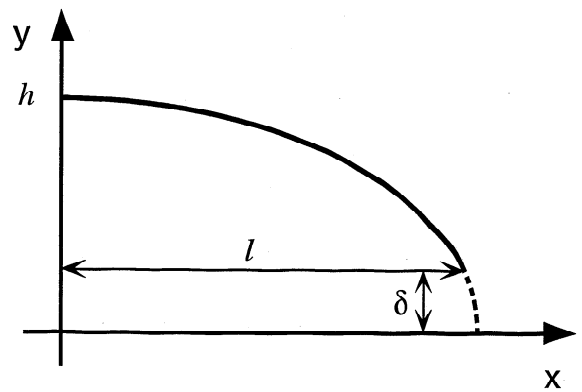

Figure A1. Assumed shape of the "rigid" dike nose used in the combined simulations intended to investigate the role of the narrow dike tip on the global flow evolution. A semiellipse having minor axis of h is truncated such that the aperture at the truncation point (assumed position of the fluid front) equals δ.

We also wished to explore the effect of the narrow tip on the flow evolution in a dike. We choose a shape of a truncated semiellipse (Figure A1) as an approximation of the mechanical thickness of the dike nose. For the majority of mid-ocean ridge dikes, the nose length is a small fraction of the thermal arrest distances, which makes it difficult to resolve it on the uniform grid used in the rigid-walled channel simulation. Therefore we use a nonlinear mapping for the along-stream coordinate, $\bar{x} = 1 - (1 - x/x_N)^{1/2}$, which stretches the region near the fluid front [e.g., *Lister*, 1994a]. Other coordinate transformations are the same as previously. At each time step, the nose is assumed to propagate preserving its mechanical shape at a constant velocity dictated by the flux from the dike tail. The contribution of the viscous pressure drop within the nose is neglected; as mentioned in section 2, coupled elastic/fluid-mechanical models indicate that the increased pressure drop necessary for flow through the narrow tip is balanced by a pressure at the magma front which is much less than the ambient value. Equations for the fluid velocities within the nose region were modified to account for the fact that the volumetric flux along the nose is not constant but varies proportionally to the nose thickness.

Acknowledgments. We thank two anonymous referees whose comments helped to improve the quality of this manuscript. This work was supported by NSF grant OCE-9617696.

References

Batiza, R., W.G. Melson, and T. O'Hearn, Simple magma supply geometry inferred beneath a segment of the Mid-Atlantic Ridge, *Nature, 335*, 428-431, 1988.

Bloomer, S.H, J.H. Natland, and R.L. Fisher, Mineral relationships in gabbroic rocks from fracture zones of Indian Ocean ridges: Evidence for extensive fractionation, parental diversity and boundary-layer recrystallization, in *Magmatism in the Ocean Basins*, edited by A.D. Saunders and M.J. Norry, *Geol. Soc. Spec. Publ., London, 42*, 107-124, 1989.

Brown, G.M., Heat or mass transfer in a fluid in laminar flow in a circular or flat conduit, *AIChE J., 6*, 179-183, 1960.

Bruce, P.M., and H.E. Huppert, Solidification and melting along dikes by the laminar flow of basaltic magma, in *Magma Transport and Storage*, edited by M.P. Ryan, pp. 87-101, John Wiley, New York, 1990.

Cannat, M., How thick is the magmatic crust at slow spreading oceanic ridges?, *J. Geophys. Res., 101*, 2847-2857, 1996.

Carslaw, H.S., and J.C. Jaeger, *Conduction of Heat in Solids*, 2nd ed., 510 pp., Oxford Univ. Press, New York, 1959.

Delaney, P.T., Heat transfer during emplacement and cooling of mafic dykes, in *Mafic Dyke Swarms*, edited by H.C. Halls and W.H. Fahrig, *Geol. Assoc. Can. Spec. Pap., 34*, 31-46, 1987.

Delaney, P.T., and D.D. Pollard, Solidification of basaltic magma during flow in dike, *Am. J. Sci., 282*, 856-885, 1982.

Detrick, R.S., P. Buhl, E. Vera, J. Mutter, J. Orcutt, J. Madsen, and T. Brocher, Multi-channel seismic imaging of a crustal magma chamber along the East Pacific Rise, *Nature, 326*, 35-41, 1987.

Dick, H.J.B., Abyssal peridotites, very slow spreading ridges and ocean ridge magmatism, In *Magmatism in the Ocean Basins*, edited by A.D. Saunders and M.J. Norry, *Geol. Soc. Spec. Publ., London, 42*, 71-105, 1989.

Dziak, R.P., C.G. Fox, and A.E. Schreiner, The June-July 1993 seismo-

acoustic event at CoAxial segment, Juan de Fuca Ridge: Evidence for a lateral dike injection, *Geophys. Res. Lett., 22,* 135-138, 1995.

Einarsson, P., and B. Brandsdottir, Seismological evidence for lateral magma intrusion during the July 1978 deflation of the Krafla volcano in NE-Iceland, *J. Geophys., 47,* 160-165, 1980.

Fedotov, S.A., Ascent of basic magmas in the crust and the mechanism of basaltic fissure eruptions, *Int. Geol. Rev., 20,* 33-48, 1978.

Fialko, Y.A., and A.M. Rubin, Numerical simulation of high pressure rock tensile fracture experiments: Evidence of an increase in fracture energy with pressure? *J. Geophys. Res., 102,* 5231-5242, 1997.

Fox, C.G., W.E. Radford, R.P. Dziak, T.-K. Lau, H. Matsumoto, and A.E. Schreiner, Acoustic detection of a seafloor spreading episode on the Juan de Fuca Ridge using military hydrophone arrays, *Geophys. Res. Lett., 22,* 131-134, 1995.

Francheteau, J., and R.D. Ballard, The East Pacific Rise near 21°N, 13°N and 20°S; Inferences for along-strike variability of axial processes, *Earth Planet. Sci. Lett., 64,* 93-116, 1983.

Gass, I.G., Magmatic processes at and near constructive plate margins as deduced from the Troodos (Cyprus) and Semail Nappe (N Oman) ophiolites, in *Magmatism in the Ocean Basins*, edited by A.D. Saunders and M.J. Norry, *Geol. Soc. Spec. Publ., London, 42,* 1-15, 1989.

Gudmundsson A., Dyke emplacement at divergent plate boundaries, in *Mafic Dykes and Emplacement Mechanisms,* edited by A.J. Parker, P.C. Rickwod and D.H. Tucker, pp. 47-62, A.A.Balkema, Brookfield, Vt., 1990.

Gudmundsson A., The geometry and growth of dikes, In *Physics and Chemistry of Dykes,* edited by G. Baer and A. Heimann, pp. 23-34, A.A.Balkema, Brookfield, Vt., 1995.

Hekinian, R., J.G. Moore, and W.B. Bryan, Volcanic rocks and process of Mid-Atlantic Ridge rift valley near 36°46'N, *Contrib. Mineral. Petrol., 58,* 83-110, 1976.

Huang, P.Y., and S.C. Solomon, Centroid depth of mid-ocean ridge earthquakes: Dependence on spreading rate, *J. Geophys. Res., 93,* 13,445-13,477, 1988.

Karson, J., et al., Along-axis variations in seafloor spreading in the MARK area, *Nature, 328,* 681-685, 1987.

Khazan, Y.M., and Y.A. Fialko, Fracture criteria at the tip of fluid driven cracks in the Earth, *Geophys. Res. Lett., 22,* 2541-2544, 1995.

Klein, F., R.Y. Koyanagi, J.S. Nakata, and W.R. Tanigawa, The seismicity of Kilauea's magma system, in *Volcanism in Hawaii,* edited by R.W. Decker, T.L. Wright, and P.H. Stauffer, *U.S. Geol. Surv. Prof. Pap., 1350,* 1019-1186,1987.

Langmuir, C.H., E.M. Klein, and T. Plank, Petrological systematics of mid-ocean ridge basalts: Constrains on melt generation beneath ocean ridges, in *Mantle Flow and Melt Generation at Mid-ocean Ridges, Geophys. Monogr. Ser.*, vol.71, edited by J.P. Morgan, D.K. Blackman and J.M. Sinton, pp. 183-280, AGU, Washington, D.C., 1992.

Lin, J., and J. Phipps Morgan, The spreading rate dependence of three-dimensional mid-ocean ridge gravity structure, *Geophys. Res. Lett., 19,* 13-16, 1992.

Lin, J., G.M. Purdy, H. Schouten, J.-C. Sempere and C. Zervas, Evidence from gravity data for focussed magmatic accretion along the Mid-Atlantic Ridge, *Nature, 335,* 627-632, 1990.

Lister, J.R., Buoyancy-driven fluid fracture: Similarity solutions for the horizontal and vertical propagation of fluid-filled cracks, *J. Fluid Mech., 217,* 213-239, 1990.

Lister J.R., The solidification of buoyancy-driven flow in a flexible-walled channel, part 1, Constant-volume release, *J. Fluid Mech., 272,* 21-44, 1994a.

Lister J.R., The solidification of buoyancy-driven flow in a flexible-walled channel, part 2, Continual release, *J. Fluid Mech., 272,* 45-65, 1994b.

Lister, J.R., and P.J. Dellar, Solidification of pressure-driven flow in a finite rigid channel with application to volcanic eruptions, *J. Fluid Mech., 323,* 267-283, 1996.

Lister, J.R., and R.C. Kerr, Fluid-mechanical models of crack propagation and their application to magma transport in dikes, *J. Geophys. Res., 96,* 10,049-10,077, 1991.

MacLeod, C.J., and D.A. Rothery, Ridge axial segmentation in the Oman ophiolite: Evidence from along-strike variations in the sheeted dyke complex, in *Ophiolites and their Modern Oceanic Analogues,* edited by L.M. Parson, B.J. Murton, and P. Browning, *Geol. Soc. Spec. Publ., London, 60,* 39-63, 1992.

Mutter, J.C., and North Atlantic Transect Study Group, Multichannel seismic images of the oceanic crust's internal structure: Evidence for a magma chamber beneath the Mesozoic Mid-Atlantic Ridge, *Geology, 13,* 629-632, 1985.

Neumann, G.A., and W.D. Forsyth, The paradox of the axial profile: Isostatic compensation along the axis of the Mid-Atlantic Ridge?, *J. Geophys. Res., 98,* 17,891-17,910, 1993.

Parsons T., and G.A. Thompson, The role of magma overpressure in suppressing earthquakes and topography: Worldwide examples, *Science, 253,* 1300-1302, 1991.

Press, W.H., S.A. Teukolsky, W.T. Vetterling, and B.P. Flannery, *Numerical Recipes: The Art of Scientific Computing,* 2nd ed., 963 pp., Cambridge Univ. Press, New York, 1992.

Rubin, A.M., A comparison of rift zone tectonics in Iceland and Hawaii, *Bull. Volcanol., 52,* 302-319, 1990.

Rubin, A.M., Dike-induced faulting and graben subsidence in volcanic rift zones, *J. Geophys. Res., 97,* 1839-1858, 1992.

Rubin, A.M., On the thermal viability of dikes leaving magma chambers, *Geophys. Res. Lett., 20,* 257-260, 1993a.

Rubin, A.M., Tensile fracture of rock at high confining pressure: Implications for dike propagation, *J. Geophys. Res., 98,* 15,919-15,935, 1993b.

Rubin, A.M., Propagation of magma-filled cracks, *Annu. Rev. Earth Planet. Sci., 23,* 287-336, 1995.

Rubin, A.M., and D.D. Pollard, Origins of blade-like dikes in volcanic rift zones, in *Volcanism in Hawaii,* edited by R.W. Decker, T.L. Wright, and P.H. Stauffer, *U.S. Geol. Surv. Prof. Pap., 1350,* 1449-1470, 1987.

Ryan, M.P., Neutral buoyancy and the mechanical evolution of magmatic systems, in *Magmatic Processes: Physicochemical Principles,* edited by B.O. Mysen, pp. 259-288, Geochem. Soc., University Park, Pa., 1987.

Schouten, H., K.D. Klitgord, and J.A. Whitehead, Segmentation of mid-ocean ridges, *Nature, 317,* 225-229, 1985.

Sigurdsson, H., and R. S. J. Sparks, Rifting episode in north Iceland in 1874-1875 and the eruptions of Askja and Sveinagja, *Bull. Volcanol., 41,* 149-167, 1978.

Sleep, N., Formation of the oceanic crust: Some thermal constraints, *J. Geophys. Res., 80,* 4037-4042, 1975.

Speight J., R. Skelhorn, T. Sloan, and R. Knaap, The dyke swarms of Scotland, in *Igneous Rocks of the British Isles,* edited by D.S. Sutherland, pp. 449-621, John Wiley, New York, 1982.

Spence, D. A., and D. L. Turcotte, Magma-driven propagation of cracks, *J. Geophys. Res., 90,* 575-580, 1985.

Thompson, G., W.B. Bryan, and S.E. Humphris, Axial volcanism on the East Pacific Rise, 10-12°N, in *Magmatism in the Ocean Basins,* edited by A.D. Saunders and M.J. Norry, *Geol. Soc. Spec. Publ., London, 42,* 181-200, 1989.

Tolstoy, M., A.J. Harding, and J.A. Orcutt, Crustal thickness on the Mid-Atlantic Ridge: Bull's-eye gravity anomalies and focused accretion, *Science, 262,* 726-729, 1993.

Walker, G.P.L., The dike complex of Koolau Volcano, Oahu: Internal structure of a Hawaiian rift zone, in *Volcanism in Hawaii,* edited by R.W. Decker, T.L. Wright, and P.H. Stauffer, *U.S. Geol. Surv. Prof. Pap., 1350,* 961-993, 1987.

Walker, G.P.L., P.R. Eyre, S.R. Spengler, M.D. Knight, and K. Kennedy, Congruent dike widths in large basaltic volcanoes, in *Physics and Chemistry of Dykes*, edited by G. Baer and A. Heimann, pp. 41-49, A.A.Balkema, Brookfield, Vt., 1995.

White, R.S., Asthenospheric control on magmatism in the ocean basins, In *Magmatism in the Ocean Basins*, edited by A.D. Saunders and M.J. Norry, *Geol. Soc. Spec. Publ., London, 42,* 17-27, 1989.

Whitehead, J.A., Jr., H.J.B. Dick, and H. Schouten, A mechanism for magmatic accretion under spreading centres, *Nature, 312,* 146-148, 1984.

Y. A. Fialko and A. M. Rubin, Department of Geosciences, Princeton University, Princeton, NJ 08544 (e-mail: fialko@geo.princeton.edu; allan@geo.princeton.edu).

(Received May 30, 1997; revised October 15, 1997;
accepted October 28, 1997.)